The Astrophysical Journal, 864:3 (11pp), 2018 September 1 https://doi.org/10.3847/1538-4357/aad45d

Determining the Kappa Distributions of Space Plasmas from Observations in a Limited Energy Range

G. Nicolaou[1,2], G. Livadiotis[3], C. J. Owen[1], D. Verscharen[1,4], and R. T. Wicks[1]
[1] Department of Space and Climate Physics, Mullard Space Science Laboratory, University College London, Dorking, Surrey, RH5 6NT, UK; g.nicolaou@ucl.ac.uk
[2] Swedish Institute of Space Physics, Kiruna, Sweden
[3] Southwest Research Institute, San Antonio, TX, USA
[4] Space Science Center, University of New Hampshire, NH, USA
Received 2018 March 7; revised 2018 June 22; accepted 2018 July 12; published 2018 August 24

Abstract

Spacecraft observations allow us to reconstruct the velocity distributions of space plasmas, which fully describe the kinetic state of the plasma. Space plasmas often exist in stationary states out of equilibrium, which are typically described by kappa distributions. Thus, the kappa index and temperature that govern these distributions are parameters that need to be determined for a full and accurate description of these plasmas. In this study, we demonstrate a novel and reliable way to determine the kappa index and temperature of plasma distribution functions constructed from counts observed in a narrow energy range by typical electrostatic sensors. Our method applies to cases in which the high-energy tail of the plasma is observed with significant uncertainty, or not observed at all. For the validation of our method, we produce pseudo-observations for typical input plasma parameters, specifically considering the design of the ion plasma instrument SWA-PAS on board the Solar Orbiter mission. Our method reliably estimates the relevant plasma parameters by fitting the angular spread of the distribution in a narrow energy range around the core bulk energy. We compare the output of our technique with the input parameters used to generate artificial data for a selected range of the kappa index and the temperature, and for a bulk energy typical for the solar wind. In addition, we study the effects of Poisson errors on the instrument's counting statistics, test our method against *Helios 2* measurements, and discuss its potential applications and limitations.

Key words: methods: data analysis – plasmas – solar wind

1. Introduction

Space plasmas have been observed for decades in many different regions of space, with a wide range of different conditions. Instruments designed to sample the plasma velocity distribution generally record the count rates for particles arriving at the instrument in a given mass, energy, and angular range. For many applications, the desired products from these plasma observations are the plasma fluid parameters, such as the bulk speed, the density, and the temperature. These higher-level products are derived from the count rates taking into account the instruments' properties, which are determined from ground and/or in-flight calibration procedures. A common method for the calculation of the plasma fluid parameters is the direct fitting of the instrument's response model to the observations, using a given expression for the plasma distribution (e.g., Richardson 1987, 2002; Wilson et al. 2008, 2012b, 2013; Elrod et al. 2012; Livi et al. 2014; Nicolaou et al. 2014, 2015a, 2015b; Elliott et al. 2016). In an alternative approach, a direct numerical integration scheme derives the velocity moments from the observed distribution function (e.g., Paschmann & Daly 1998; Wilson et al. 2012a). This method requires that the full distribution function be within the energy and angular range of the instrument (see also Kasper et al. 2006).

Plasmas in collisional equilibrium exhibit a Maxwellian distribution. Space plasmas, however, are very often in stationary states out of equilibrium that can be described by kappa distributions. Kappa distributions are characterized by a Maxwellian-like "core" (velocities close to the bulk velocity of the distribution function) and a high-energy tail that follows a power law. They have been observed in the solar wind (e.g., Maksimovic et al. 1997, 2005; Pierrard et al. 1999; Chotoo et al. 2000; Mann et al. 2002; Zouganelis et al. 2004; Marsch 2006; Štverák et al. 2009; Livadiotis & McComas 2013b; Yoon 2014; Heerikhuisen et al. 2015; Pierrard & Pieters 2014), planetary magnetospheres (e.g., Christon 1987; Collier & Hamilton 1995; Jurac et al. 2002; Pisarenko et al. 2002; Kletzing et al. 2003; Mauk et al. 2004; Schippers et al. 2008; Dialynas et al. 2009; Ogasawara et al. 2013; Carbary et al. 2014; Qureshi et al. 2014; Stepanova & Antonova 2015), the outer heliosphere, and the inner heliosheath (e.g., Decker & Krimigis 2003; Decker et al. 2005; Heerikhuisen et al. 2008, 2010; Zank et al. 2010; Livadiotis et al. 2011, 2012, 2013; Livadiotis & McComas 2011a, 2012), and have been studied in other various plasma-related analyses (e.g., Milovanov & Zelenyi 2000; Saito et al. 2000; Yoon et al. 2006; Raadu & Shafiq 2007; Hellberg et al. 2009; Livadiotis 2009, 2014, 2015b, 2015c, 2016a, 2016b; Livadiotis & McComas 2009, 2010a, 2010b, 2011b, 2013c; Tribeche et al. 2009; Baluku et al. 2010; Le Roux et al. 2010; Eslami et al. 2011; Kourakis et al. 2012; Fisk & Gloeckler 2014; Randol & Christian 2014; Varotsos et al. 2014; Liu et al. 2015; Viñas et al. 2015). Furthermore, several studies (e.g., Milovanov & Zelenyi 2000; Leubner 2002; Livadiotis & McComas 2009; Livadiotis 2015a) have shown that the kappa distributions arise naturally from Tsalis nonextensive statistical mechanics (Tsallis 1988, 2009; Tsallis et al. 1998). For other examples of kappa-distributed

plasmas, see Livadiotis (2017) and references therein. Previous studies have shown that fitting a Maxwellian distribution to the core of a kappa distribution can lead to major misestimations in the plasma temperature (Livadiotis & McComas 2009, 2013a; Nicolaou & Livadiotis 2016). Therefore, a careful treatment of the kappa distribution is important, taking into account the contribution of particles with velocities in the tail of the distribution. The Maxwellian distribution is the limit of the kappa distribution for $\kappa \to \infty$. Therefore, the use of kappa distributions includes the identification of Maxwellian distributions. We note that the kappa index is an additional free parameter for the distribution that has to be determined.

In practice, however, high-energy tails are not always observed due to instrumental constraints. For example, the plasma instrument on board *Voyager 2* provides observations of only a few data points in a limited energy range, which complicates the determination of the distribution-function fit parameters (e.g., Scherer et al. 2018). In addition, there are cases in which two or more plasma populations overlap within the instrument's energy range. For example, Nicolaou et al. (2014) report that it is not possible to clearly distinguish the high-energy tail of the Jovian magnetosheath proton distribution due to the overlap with the alpha particle distribution. In such cases, the necessity for an alternative method to determine kappa distributions arises, especially one that can be usefully applied using a limited range of energies and angles so that, for example, different species of particles can be excluded. We present such a method to generate reliable and efficient determinations of plasma bulk parameters when the full distribution is not accessible.

This paper is organized as follows: In Section 2, we introduce a new method to estimate the kappa index and temperature of kappa distribution functions by analyzing data obtained in a limited energy and angular range around the energy and direction associated with the plasma bulk flow. In Section 3, we validate our method, considering the expected observations of the SWA-PAS instrument on board Solar Orbiter, which can adopt our method for on-board processing in the future. In Section 4, we apply our method to three ion distributions observed by *Helios 2* at heliocentric distances between ~0.4 and ~0.7 au. In Section 5, we discuss the results and we summarize our conclusions.

2. Method

The goal of our study is to determine the kappa index and the plasma temperature of kappa-distributed particles when observations are only available in a narrow energy range and a narrow azimuth range. Therefore, we consider plasma particle populations with an isotropic (in temperature and particle correlation) kappa distribution function:

$$f(\boldsymbol{u}) = n(\pi u_{\rm th}{}^2)^{-\frac{3}{2}} A_\kappa \cdot \left[1 + \frac{(|\boldsymbol{u} - \boldsymbol{u}_0|)^2}{\left(\kappa - \frac{3}{2}\right) u_{\rm th}{}^2}\right]^{-\kappa-1}, \quad (1a)$$

where:

$$A_\kappa = \left(\kappa - \tfrac{3}{2}\right)^{-\frac{3}{2}} \frac{\Gamma(\kappa+1)}{\Gamma\left(\kappa - \frac{1}{2}\right)}. \quad (1b)$$

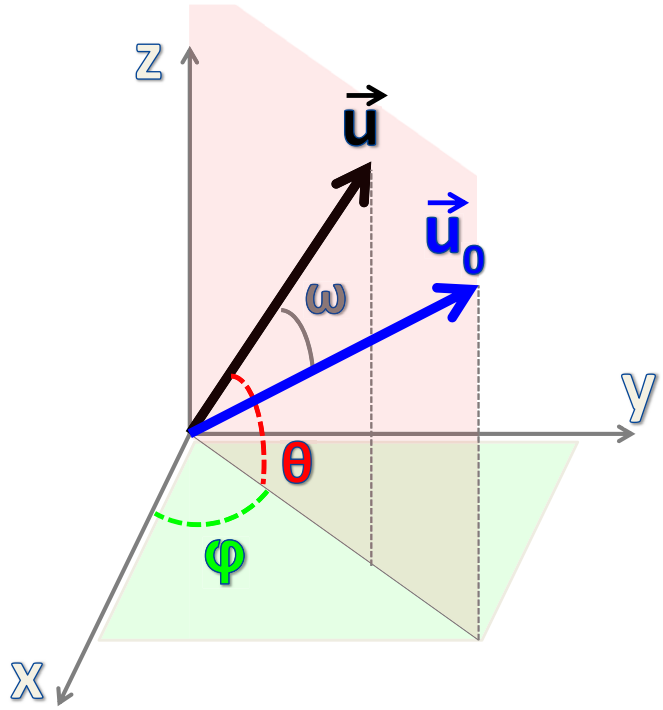

Figure 1. Coordinate system we use in this study. The elevation angle θ measures the angle of a particle velocity vector (black arrow) from the x–y plane (increasing toward the z-axis) while the azimuth angle φ is the angle between the x-axis and the projection of the velocity vector on the x–y plane (measured from the x-axis and increasing toward the y-axis). The bulk velocity vector is represented with the blue vector. We illustrate a case in which the particle velocity has the same azimuth as the bulk velocity vector, so that the two vectors lie within the same plane (red shadowed plane). Then the ω angle between the two vectors corresponds to the difference between the measurement elevation angle for a particular bin and the measured elevation angle of the bulk velocity bin.

The distribution is a function of the particle velocity $\boldsymbol{u}$. In the above equation, n is the density, $u_{\rm th} = \sqrt{2k_{\rm B}T/m}$ is the thermal speed, $k_{\rm B}$ is the Boltzmann constant, T is the temperature, m is the mass of a particle of the species, $\boldsymbol{u}_0$ is the bulk velocity, Γ is the gamma function, and κ is the kappa index of the distribution function with values between $3/2$ and infinity. In this formulation, T is the second velocity moment of the distribution function and does not depend on κ. In the limit $\kappa \to \infty$ the distribution asymptotes toward the Maxwellian distribution. In the limit $\kappa \to 3/2$, the distribution describes plasma in the state furthest from the classical thermal equilibrium (anti-equilibrium—for more details, see Livadiotis & McComas 2010a, 2013a; Livadiotis 2015a). The normalization is such that the distribution satisfies:

$$\frac{1}{n}\int_{-\infty}^{+\infty} f(\boldsymbol{u}) d^3\boldsymbol{u} = 1. \quad (1c)$$

We rewrite Equation 1(a) in terms of the particle kinetic energy $\varepsilon = \frac{1}{2}m\,|\boldsymbol{u}|^2$ and the bulk energy $E_0 = \frac{1}{2}m\,|\boldsymbol{u}_0|^2$:

$$f(\varepsilon, \omega) = N\left[1 + \frac{\varepsilon + E_0 - 2\sqrt{\varepsilon E_0}\cos\omega}{\left(\kappa - \frac{3}{2}\right)k_{\rm B}T}\right]^{-\kappa-1}, \quad (2)$$

where ω is the angle between the particle velocity $\boldsymbol{u}$ and the bulk velocity $\boldsymbol{u}_0$ vector, and is a function of the elevation θ and

the azimuth φ angle of the spherical coordinate system (see Figure 1). In Equation (2), N is a normalization factor.

We now limit our analysis to a range of elevations θ at a specific energy and azimuth that includes the part of the distribution of particles at both the energy E_0 and the azimuth direction φ_0 of the bulk plasma flow. We directly determine E_0 and the azimuth direction φ_0 as the peak of the distribution function in the data matrices. For the special case in which $\varepsilon = E_0$, Equation (2) becomes:

$$f(\omega) = N\left[1 + \frac{2E_0(1 - \cos\omega)}{\left(\kappa - \frac{3}{2}\right)k_B T}\right]^{-\kappa-1}, \quad (3)$$

which for a given distribution is a function of ω only. If we further consider only the particles with $\varphi = \varphi_0$, then ω simply represents the difference of the particle elevation θ and the bulk velocity elevation direction θ_0 (see Figure 1). Equation (3) then becomes:

$$f(\varepsilon = E_0, \theta, \varphi = \varphi_0) = N\left[1 + \frac{2E_0(1 - \cos(\theta - \theta_0))}{\left(\kappa - \frac{3}{2}\right)k_B T}\right]^{-\kappa-1}, \quad (4)$$

which is a function of the elevation angle only and can be fitted to the one-dimensional (1D) distribution obtained in one full elevation scan at the bulk energy and azimuth of the bulk. Electrostatic sensors usually perform elevation-angle scans in discrete energy and azimuth bins. Therefore, we directly obtain the 1D distribution at E_0 and φ_0 from the observations. We note that the specific method requires that the fitting routine successfully identifies the dependence of the observed distribution on the elevation direction, which is not the c ase when $E_0/k_B T \ll 1$. For solar-wind protons, however, $E_0/k_B T \gg 1$, allowing accurate fits to the 1D elevation scans. The free parameters of the fitting are the normalization factor N, the elevation of the bulk θ_0, the kappa index κ and the plasma temperature T. We determine the factor N and the elevation of the bulk θ_0 directly from the observed data as the peak value of the distribution and the elevation scan at which the peak is observed. For this study, we leave them as free parameters for a better adjustment of the fitted curve.

3. Validation

3.1. SWA-PAS Model

We develop a model of the SWA-PAS sensor response for a given plasma distribution and then analyze the modeled observations with our method. The SWA-PAS sensor consists of an electrostatic analyzer designed to make high temporal resolution measurements of the solar-wind protons in the energy-per-charge range from ~0.2 keV/q to 20 keV/q. This energy range is resolved in 96 steps, with an energy resolution of $\Delta E/E = \sim 0.075$. The field of view (FOV) covers angles from −22°.5 to +22.5° in elevation and from −24° to +42° in azimuth with respect to the direction of the Sun, through 9 sectors (using deflector plates) with ~5° resolution in elevation and 11 physical sectors (~6° each) in azimuth (Figure 2).

We create artificial SWA-PAS data for a given input plasma distribution, f, as proton counts per specific-energy and solid-angle element, $C(E, \Theta, \Phi)$, as

$$C(E, \Theta, \Phi) = \frac{2\Delta\tau}{m^2} \cdot \int_{E-\frac{1}{2}\Delta E}^{E+\frac{1}{2}\Delta E} \int_{\Theta-\frac{1}{2}\Delta\Theta}^{\Theta+\frac{1}{2}\Delta\Theta} \int_{\Phi-\frac{1}{2}\Delta\Phi}^{\Phi+\frac{1}{2}\Delta\Phi} \times A_{\rm eff}(\varepsilon, \theta, \varphi) f(\varepsilon, \theta, \varphi)\varepsilon d\varepsilon \sin\theta d\theta d\varphi, \quad (5)$$

where E, Θ, and Φ are the bin-centered discrete energy, elevation, and azimuth coordinates of the instrument, respectively, corresponding to the detected particle energy and direction that is opposite to the instrument's viewing direction. $\Delta\tau$ is the integration time, m is the proton mass, and $A_{\rm eff}$ is the effective aperture of the instrument, which is in general a function of the energy and direction of the detected particles. The limits of the above integral are defined by the instrument's energy resolution and the angular resolution (in the case of PAS these are $\Delta E/E = 0.075$, $\Delta\Theta = 5°$, $\Delta\Phi = 6°$ respectively). For simplicity, we assume that $A_{\rm eff}$ does not vary within an elevation bin and is a discrete function proportional to $\sin^{-1}\Theta$ only, i.e., $A_{\rm eff}(\varepsilon, \theta, \varphi) \equiv A_{\rm eff}(\Theta) = A_0 / \sin\Theta$. A more realistic response will be assessed when the full flight calibration of the instrument is completed. Under the current assumption, our model Equation (5) simplifies to:

$$C(E, \Theta, \Phi) = \frac{2\Delta\tau A_0}{m^2 \sin\Theta} \int_{E-\frac{1}{2}\Delta E}^{E+\frac{1}{2}\Delta E} \int_{\Theta-\frac{1}{2}\Delta\Theta}^{\Theta+\frac{1}{2}\Delta\Theta} \int_{\Phi-\frac{1}{2}\Delta\Phi}^{\Phi+\frac{1}{2}\Delta\Phi} \times f(\varepsilon, \theta, \varphi)\varepsilon d\varepsilon \sin\theta d\theta d\varphi. \quad (6)$$

In a realistic measurement, the instrument provides us with $C(E, \Theta, \Phi)$, and our goal is the determination of the underlying velocity distribution function. We achieve this goal by inverting Equation (6) in order to determine a (discrete) approximation $f_{\rm out}(E, \Theta, \Phi)$ of the underlying distribution function. From Equation (6), using the approximation of small ΔE, $\Delta\Theta$, and $\Delta\Phi$, we find:

$$C(E, \Theta, \Phi) \approx \frac{2}{m^2}\Delta\tau A_0 f(\varepsilon = E, \theta = \Theta, \varphi = \Phi) \times E\Delta E\Delta\Theta\Delta\Phi, \quad (7)$$

leading to the discrete (output) distribution function as a function of the observed counts:

$$f_{\rm out}(E, \Theta, \Phi) \approx \frac{m^2 C(E, \Theta, \Phi)}{2GE^2}, \quad (8)$$

where $G = \Delta\tau A_0 \frac{\Delta E}{E}\Delta\Theta\Delta\Phi$ is the geometric factor of the instrument.

To demonstrate the use of our model, we numerically integrate Equation (6) using a Riemann integration algorithm. We choose small enough integration steps ($d\varepsilon$, $d\theta$, $d\varphi$) to reach convergence of the output parameters. We model the counts for each energy scan E, in each elevation scan Θ, in each azimuth sector Φ, and for specific integration time $\Delta\tau$. We construct pseudo-observations as counts in an elevation-energy matrix (integrated over azimuth) and in an azimuth-energy matrix (integrated over elevation). In Figure 3, we show both matrices for plasma protons described by a kappa distribution with bulk energy $E_0 = 1$ keV, temperature $T = 40$ eV, and a kappa index $\kappa = 3$.

We then derive the distribution function $f_{\rm out}$ from the observed counts with Equation (8). This result is shown in Figure 4 as matrices of the distribution function, using the same parameters as in the proton example shown in Figure 3.

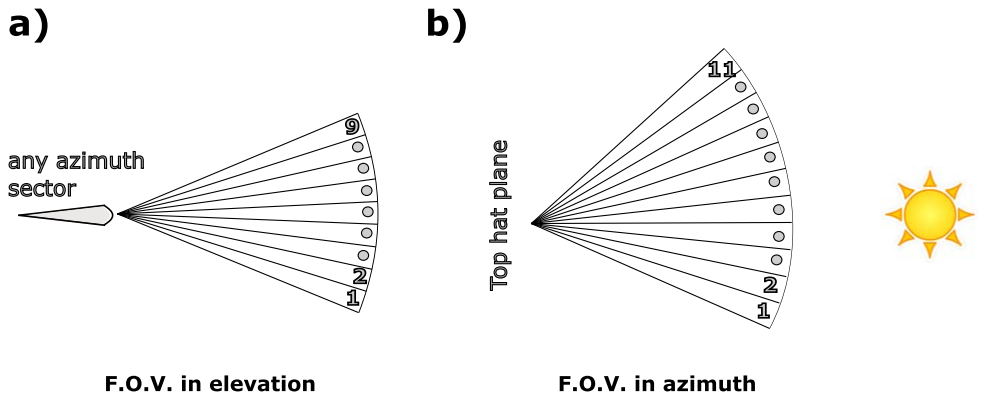

Figure 2. Field of view (FOV) of the SWA-PAS instrument: (a) The elevation FOV covers angles from $-22.^{\circ}5$ to $+22.^{\circ}5$ with respect to the Sunward direction through nine electrostatic sectors with a resolution of $\sim 5^{\circ}$. (b) The azimuth FOV covers angles from -24° to $+42^{\circ}$ with respect to the Sunward direction through 11 azimuth sectors (physical sectors of the instrument) with a resolution of $\sim 6^{\circ}$.

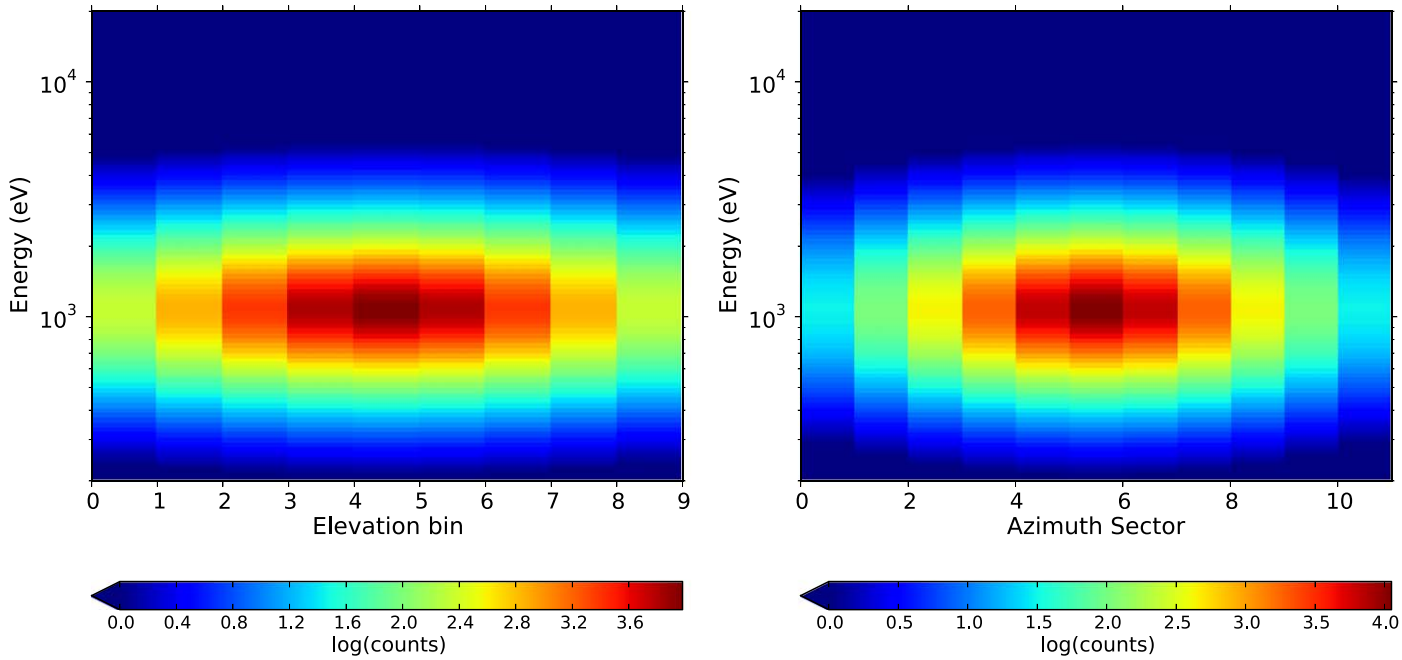

Figure 3. (Left) Elevation-energy matrix and (right) azimuth-energy matrix of SWA-PAS pseudo-observations for protons with bulk energy $E_0 = 1$ keV, temperature $T = 40$ eV, and a $\kappa = 3$.

In order to apply our method to the produced SWA/PAS pseudo-observations, we first identify the specific energy $E_{\max}$ and the azimuth sector $\Phi_{\max}$ for which $f_{\rm out}$ has its peak (see also Figure 4). These are approximately the energy E_0 and azimuth φ_0 of the bulk flow respectively. We then select the part of $f_{\rm out}$ found in the elevation bins with $E = E_{\max}$ and $\Phi = \Phi_{\max}$. The resulting 1D elevation profile is then directly fitted to Equation (4), returning an estimation of the output kappa index $\kappa_{\rm 1D}$ and plasma temperature $T_{\rm 1D}$. We present two examples for these fits at $E = E_{\max}$ and $\Phi = \Phi_{\max}$ in Figure 5.

Because of the instrument's limited energy and angular resolution, the plasma parameters derived using our method deviate to some extent from those of the underlying distribution. We quantify this systematic error (deviation between the input and the method output) by examining the ratio between the fitted kappa and the input kappa ($\kappa_{\rm 1D}/\kappa$) as well as the ratio between the fitted temperature and the input temperature ($T_{\rm 1D}/T$) for a range of input values for kappa (κ) and temperatures (T) in Figure 6. The results of our method may also depend on the plasma bulk energy E_0. In this example, however, we set the plasma bulk energy to $E_0 = 1$ keV, which is representative of slow solar-wind protons.

3.2. Poisson Statistics

Counting statistics introduce uncertainties to particle measurements in electrostatic analyzers that follow the Poisson distribution. The Poisson error for a measurement of C counts has an uncertainty of $\delta C = \pm\sqrt{C}$ counts. In order to determine the effect of counting statistics on the accuracy of our method, we follow the procedure described in Section 3, but with $C(E, \Theta, \Phi)$ randomly selected from the Poisson distribution with an expectation value given by Equation (6). We repeat this procedure 500 times for each set of κ and T and study histograms of the derived $\kappa_{\rm 1D}$ and $T_{\rm 1D}$.

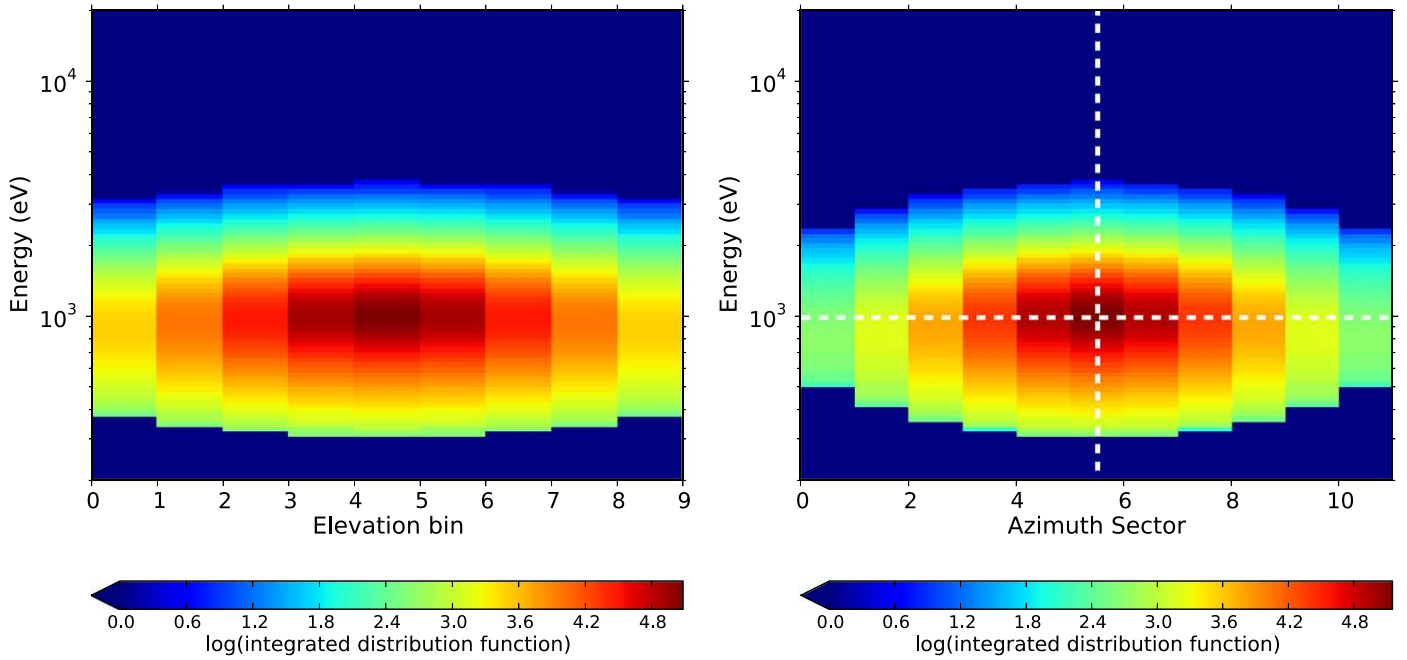

Figure 4. Distribution function normalized to its minimum (excluding zeros), of plasma protons with $E_0 = 1$ keV, thermal energy $T = 40$ eV, and $\kappa = 3$ presented as a function of elevation and energy, integrated over azimuth (left) and as function of azimuth and energy, integrated over elevation (right), as derived with Equation (8) from the pseudo-counts shown in Figure 3. The horizontal (vertical) dashed line shows the energy bin $E_{\max}$ (azimuth bin $\Phi_{\max}$) of the distribution's maximum.

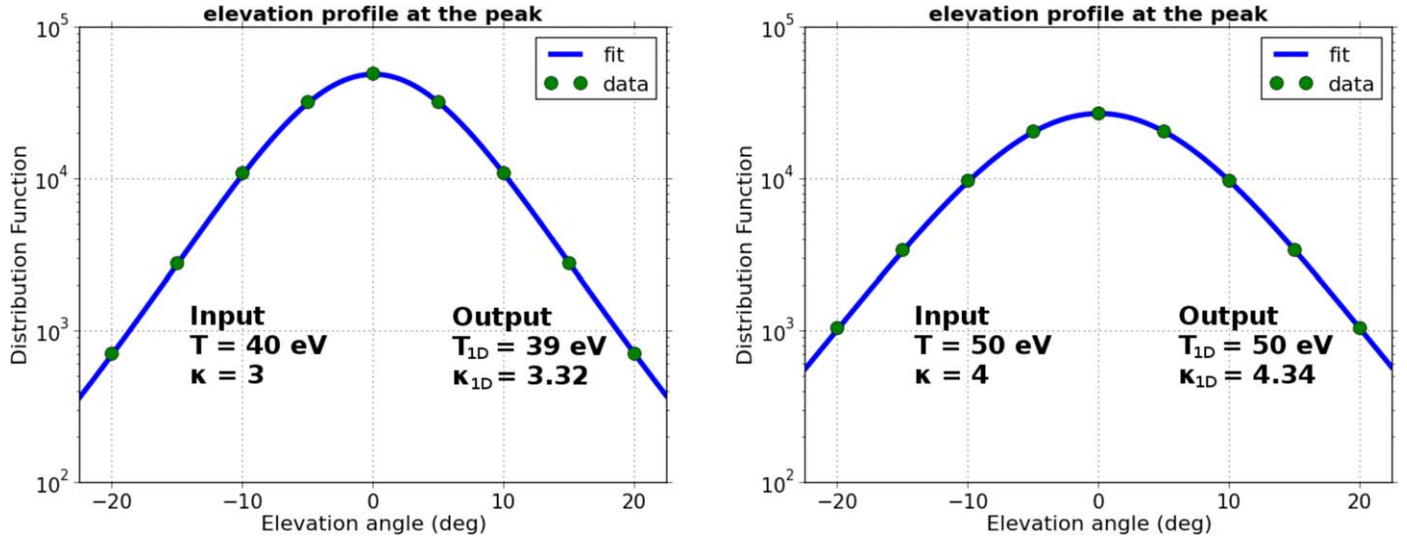

Figure 5. Fits of the 1D elevation profiles of the distribution function at the energy bin $E = E_{\max}$ and azimuth bin $\Phi = \Phi_{\max}$ for the artificial SWA-PAS data. These bins approximately represent the energy E_0 and azimuth φ_0 of the bulk flow velocity. The underlying pseudo-observations have (left) $\kappa = 3$, $E_0 = 1$ keV, $T = 40$ eV and (right) $\kappa = 4$, $E_0 = 1$ keV and $T = 50$ eV. These input parameters and the corresponding output parameters κ_{1D} and T_{1D} are shown on the left- and right-hand sides of the plot respectively.

We show two examples for such histograms in Figure 7, in which we apply our method to observations that have a peak at ~4000 counts. In this example, ~70% of the pseudo-observation analyses with Poisson error derive a kappa index within 25% of the true value. This fraction is even higher (~90%) for the temperature. Consequently, even though counting noise has an impact on the accuracy of our method, the actual SWA-PAS observations will allow the successful use of our method. When applying our method to data sets with a greater number of counts than the counts of this example, the relative Poisson error is smaller, increasing the accuracy of the derived parameters.

3.3. Statistical Verification for the Fixed Parameters E_0 and φ_0

In this subsection, we verify that the 1D elevation profile of a distribution function obtained at the energy channel $E = E_{\max}$ and azimuth sector $\Phi = \Phi_{\max}$, is a good approximation to the elevation profile of the distribution function at $\varepsilon = E_0$ and $\varphi = \varphi_0$. In order to demonstrate that, we fit Equation (2), which is the full three-dimensional (3D) distribution equation, to the truncated data set selected at $E = E_{\max}$ and $\Phi = \Phi_{\max}$. We let the bulk energy E_0 and the azimuth direction of the bulk velocity φ_0 as free parameters to be estimated by the best fit. In Figure 8, we show such a fit to a pseudo-observation with input $E_0 = 1$ keV,

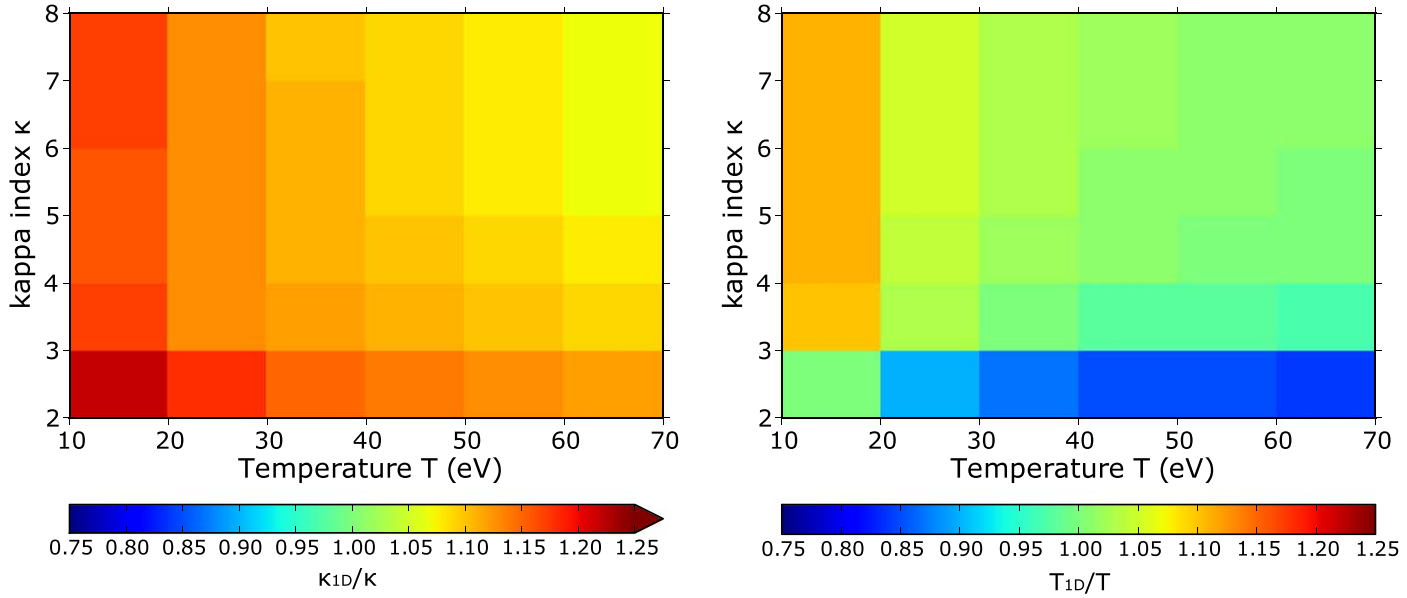

Figure 6. (Left) Ratio, κ_{1D}/κ, between the fitted kappa index, κ_{1D}, and the input kappa index, κ, as a function of the input κ and T. (Right) Ratio, T_{1D}/T, between the fitted temperature, T_{1D}, and the input temperature, T, as functions of the input κ and T in our analysis of SWA-PAS pseudo-observations. Both κ_{1D} and T_{1D} show smaller deviations from the input parameters for higher κ and T. In general, our method overestimated the kappa index over the range of the examined input parameters. The overestimation can be up to ∼25% for the smallest kappa and lowest temperature tested ($\kappa = 2$, $T = 10$ eV) but it can be as low as ∼7% for higher kappa and temperature ($\kappa = 7$, $T = 60$ eV). The plasma temperature is returned with lower uncertainty (<12%) for the range of the input parameters and the bulk speed we consider here.

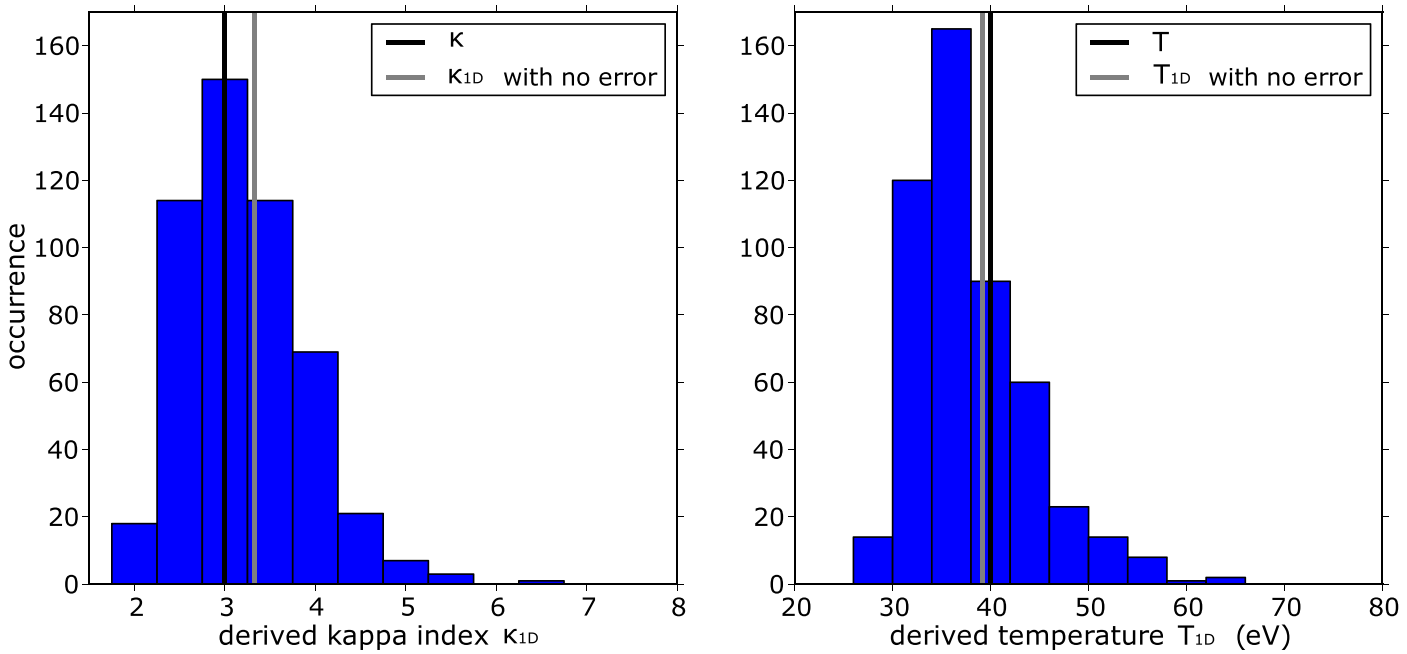

Figure 7. Histograms of (left) the derived kappa index κ_{1D} and (right) the derived plasma temperature T_{1D} using our method of pseudo-observations with Poisson-distributed random pseudo-counts for a plasma with $E_0 = 1$ keV, $T = 40$ eV, and $\kappa = 3$. For this statistical analysis, we evaluate our method 500 times to pseudo-observations with a peak at ∼4000 counts. The black lines show the input values while the gray lines indicate the output values without Poisson uncertainty is introduced in the counts. For the specific example 70% of the pseudo-observations estimate the kappa index within 25% of its true value and 90% estimate the temperature within 25% of its true value.

$\varphi_0 = 9°$, $T = 30$ eV, and $\kappa = 4$. The fitting method derives $E_{0\text{fit}} \approx 1.08$ keV, $\varphi_{0\text{fit}} \approx 10.^{\circ}8$, $T_{\text{fit}} = 31$ eV, and $\kappa_{\text{fit}} = 4.44$. The differences between the input bulk energy and azimuth direction of the bulk velocity values (E_0 and φ_0) and the corresponding fitting results (E_{ofit} and $\varphi_{0\text{fit}}$) are of the order of the instrument's energy and angular resolution respectively. Nevertheless, the derived temperature and kappa index (T_{fit} and κ_{fit}) are nearly identical to those derived by our method (T_{1D} and κ_{1D}) by fitting the simplified Equation (4) to the truncated data set assuming that $E_{\max}$ and $\Phi_{\max}$ approximately represent the energy E_0 and azimuth φ_0 of the bulk flow velocity respectively.

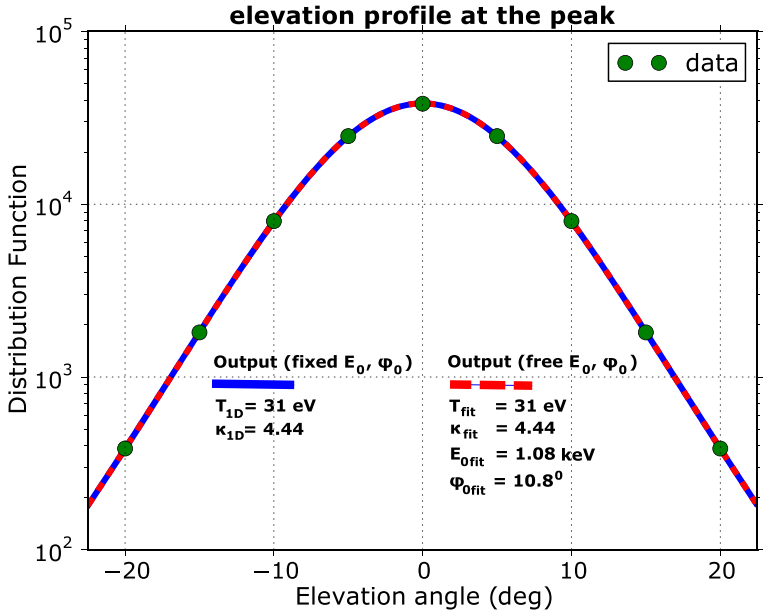

Figure 8. The 1D elevation profile of a modeled distribution obtained at the energy bin $E = E_{\max}$ and azimuth bin $\Phi = \Phi_{\max}$ of the SWA-PAS (green circles) and two different fits to the pseudo-data; a fit of Equation (4) with four free parameters (N, θ_0, T, and κ; blue line), which is a direct application of our method, and a fit of Equation (2) with six free parameters (N, E_0, θ_0, φ_0, T, and κ; red dashed line). The second fit estimates the energy and the azimuth direction of the bulk velocity within the order of the instrument's resolution, verifying the assumption $E_{\max} \approx E_0$ and $\Phi_{\max} \approx \varphi_0$. Note also, that both fits derive nearly identical plasma temperature and kappa index. In the specific example, the underlying pseudo-observation has $E_0 = 1$ keV, $T = 30$ eV, and $\kappa = 4$.

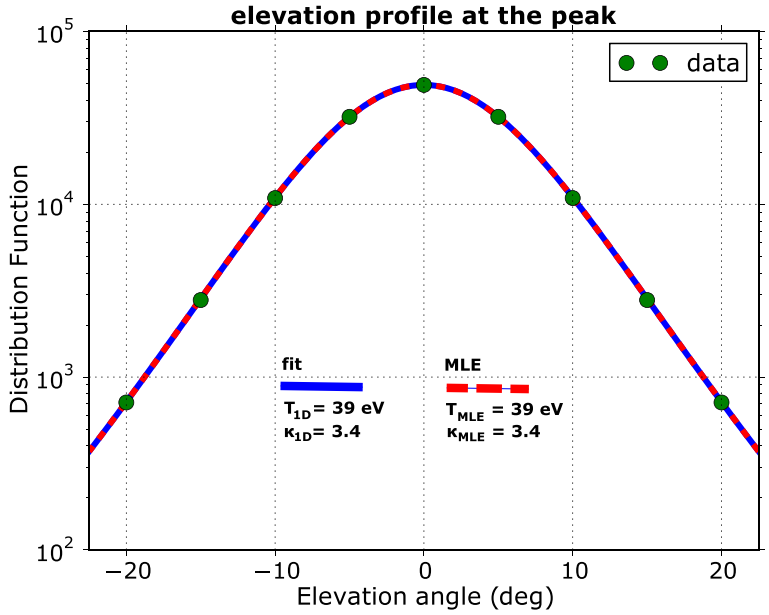

Figure 9. Reduced 1D elevation profile of a modeled distribution at $E = E_{\max}$ and $\varphi = \varphi_{\max}$ (green circles) along with the curves as estimated by the best-fit method (blue line) and the MLE method (red dashed line). The underlying pseudo-observation has $\kappa = 3$, $E_0 = 1$ keV, $T = 40$ eV. Both the fitting and the MLE method derive the same temperature $T_{1D} = T_{MLE} = 39$ eV and the same kappa index $\kappa_{1D} = \kappa_{MLE} = 3.4$.

3.4. *Comparison with the Maximum Likelihood Estimation Method (MLE)*

In our analysis, we estimate T_{1D} and κ_{1D} by fitting the reduced data sets to Equation (4). However, a future user may use another approach to analyze the 1D elevation profiles of the distributions. In this subsection, we apply the MLE method (e.g., Lawless 2011) to some of the reduced data sets in order to derive the plasma temperature T_{MLE} and kappa index κ_{MLE}, and we then compare them with the fitting results, T_{1D} and κ_{1D} respectively. Figure 9 shows the 1D elevation profile of a simulated distribution for $E_0 = 1$ keV, $T = 40$ eV, and $\kappa = 3$, and the corresponding elevation profiles from the fitting method and the MLE method. Both methods yield $T_{MLE} = T_{1D} \approx 39$ eV and $\kappa_{MLE} = \kappa_{1D} \approx 3.4$. The comparison shows that the two methods derive essentially the same plasma temperature and kappa index for a wide range of the input plasma parameters we consider in this study (see Section 3.1).

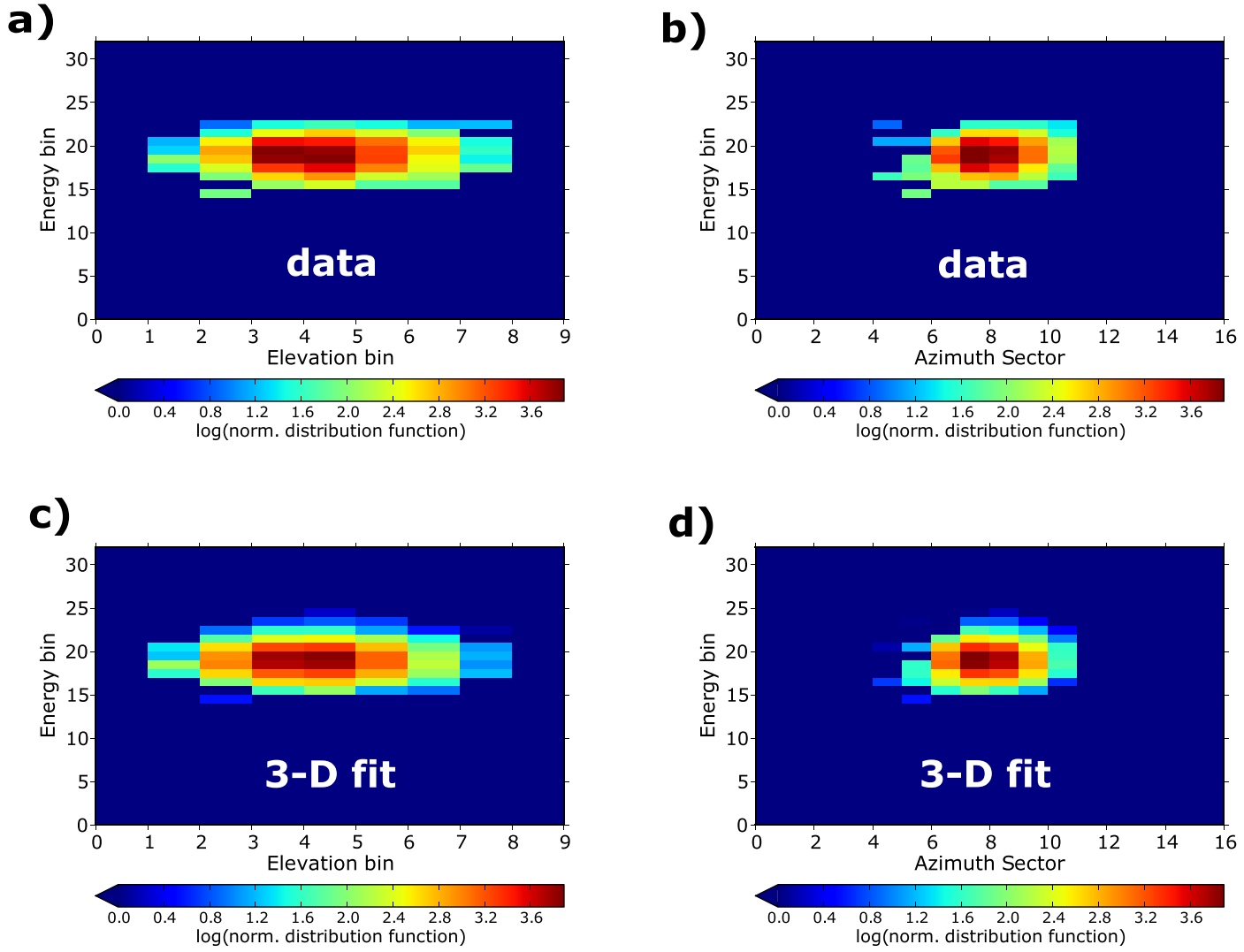

Figure 10. (a) The elevation-energy matrix and (b) the azimuth-energy matrix of the proton distribution function observed by *Helios 2* on day 67 of year 1976 at 22:32:33 UT. (c) The elevation-energy and (d) the azimuth-energy matrix of the 3D isotropic kappa distribution fit.

We note, however, that the results of the two methods deviate when applied to 1D distributions in the cold ($T < 20$ eV) and/or low kappa index ($\kappa < 3$) range. For instance, when applied to a distribution with $E_0 = 1$ keV, $T = 10$ eV, and $\kappa = 2$, the fitting yields $T_{1D} \approx 10$ eV and $\kappa \approx 2.4$, while the MLE method yields $T_{MLE} \approx 8$ eV and $\kappa_{MLE} \approx 3.2$. In general, the fitted curve describes the "tails" of the elevation profiles more accurately in this low T and low κ range. We recommend to apply similar validation methods whenever an alternative statistical approach is chosen to determine the plasma temperature and kappa index.

4. Application to *Helios 2* Data

We now illustrate our method by applying it to a real data set from the *Helios* spacecraft. The 3D electrostatic ion analyzer on board *Helios* (Schwenn et al. 1975; Rosenbauer et al. 1977) was designed to observe the velocity distributions of solar-wind ions between 0.3 and 1 au. A full 3D distribution was nominally obtained every 40 s, within the energy-per-charge range from 0.155 to 15.3 keV/q, resolved in 32 exponentially distributed energy channels. The FOV consisted of 9 elevation channels and 16 azimuth channels with approximately $5° \times 5°$ resolution. Marsch et al. (1982; referred to as M82 in this paper) present a survey of proton velocity distribution functions observed by the *Helios* probes and calculate the corresponding plasma parameters from the moments of the observed distributions by integration. We use some of M82's published measurements as test cases for our method. We choose three of the most isotropic distributions from their work. We then compare the kappa index κ_{1D} and temperature T_{1D} derived by our method with the values we obtain by fitting the entire 3D distribution (κ_{3D} and T_{3D}) to Equation (1) and with the integrated temperature values given by M82 (as the temperature $T_{||}$ parallel with respect to the magnetic field and the temperature $T_{\perp}$ perpendicular to the magnetic field). Figure 10 shows the proton distribution function observed by *Helios 2* on day 67 of year 1976 at 22:32:33 UT. The upper panels show the elevation-energy and the azimuth-energy matrices of the observed distribution, and the lower panels show the results of our 3D isotropic kappa distribution fit to the observations. We apply our 1D fitting method at $E = E_{max}$ and $\Phi = \Phi_{max}$ as described in Section 2 and show the result in Figure 11. Table 1 shows the derived parameters and those given by M82 for the three distributions we analyze.

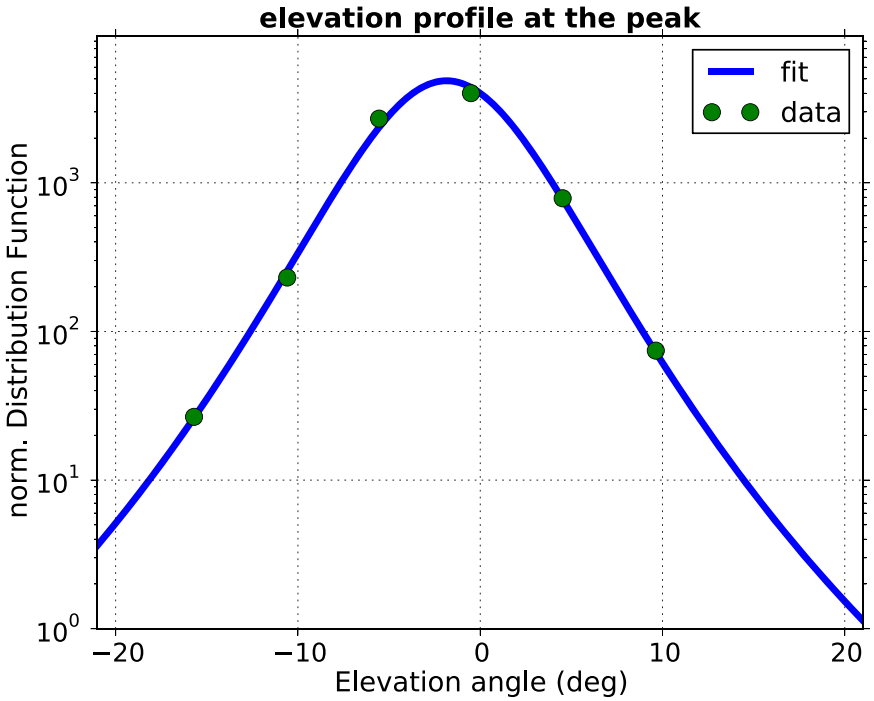

Figure 11. Fit of the 1D cut of the distribution function shown in Figure 9 at the energy $E = E_{max}$ and azimuth $\Phi = \Phi_{max}$.

Table 1
Parameters of the Three Distribution Functions Observed by *Helios 2* and Analyzed in This Work

Name in M82	Day, 1976	Time, UT	R, au	κ_{1D}	κ_{3D}	$T_{1D}(10^5$ K)	$T_{3D}(10^5$ K)	$T_{\parallel}$ (10^5 K)	$T_{\perp}$ (10^5 K)
F	67	22:32:33	0.742	2.9 (±0.3)	2.7 (±0.4)	3.63 (±0.25)	4.43 (±0.30)	3.13	3.30
C2	77	13:32:14	0.639	3.6 (±0.5)	3.6 (±0.9)	2.56 (±0.15)	2.90 (±0.50)	3.99	3.19
G	122	01:57:09	0.421	65.8 ($\kappa_{1D} > 20$)	15.3 ($\kappa_{3D} > 10$)	0.75 (±0.03)	0.78 (±0.04)	0.75	0.80

Note. The fitting errors are given in parentheses.

Both the 1D and the 3D distribution fits suggest that the first two distributions, denoted as F and C2, are kappa distributions with low kappa index ($\kappa < 4$). For distribution F, the derived κ_{1D} is by ∼10% greater than the derived κ_{3D} index, but κ_{1D} and κ_{3D} are equal to the first decimal figure for distribution C2. Both fits give very large values for kappa ($\kappa > 15$) for distribution G, suggesting that the specific distribution is practically a Maxwellian. For distribution F, both the 1D and the 3D fits give higher temperatures than those derived by M82. On the other hand, for distribution C2, the fit temperatures are smaller than those given by M82. We discuss possible reasons for this deviation in Section 5. For distribution G, the derived T_{1D} and T_{3D} lie within 5% of the values derived by M82.

5. Discussion and Conclusions

We present a method to estimate the kappa index and temperature of space plasma populations assuming an isotropic kappa velocity distribution based on measurements from a sensor observing discrete sectors in azimuth, elevation, and energy. Our method estimates the plasma parameters by analyzing just part of the observed distribution. It is, therefore, successful in cases in which the high-energy tails of the distribution overlap with the distributions of other species, or in cases in which they are not observed at all due to energy-range limitations of the instrument. Our method first determines the approximate bulk velocity (energy and direction) from the distribution's peak. We then fit the distribution as a function of the instrument elevation angle at the energy and azimuth coordinates of the bulk velocity. This choice simplifies the fitting by reducing the number of free parameters.

To illustrate and validate our method, we first model the expected response of the SWA-PAS instrument on board Solar Orbiter, which is designed to measure the velocity distribution functions of the solar-wind protons at heliocentric distances between 0.3 and 1 au. Using the instrument's characteristics (such as FOV, sensitivity, and energy resolution), we construct realistic pseudo-observations like those expected from SWA-PAS when the plasma is kappa-distributed. Then, we derive the kappa index and the temperature of the distribution by fitting the elevation profile. For verification, we compare the results of our method with the input of the pseudo-observations. We conclude that:

(i) In general, our method successfully estimates the kappa index and the temperature of the solar-wind protons from data obtained at the energy channel and the azimuth sector of the distribution's maximum by the SWA-PAS sensor (or similar design).

(ii) The systematic error of the derived kappa index and temperature depends on the plasma parameters: it decreases as the kappa index and the temperature increase. For example, for a bulk energy of $E_0 = 1$ keV, the kappa

index is overestimated by ∼25% when the method is applied to plasma with $\kappa = 2$ and $T = 10$ eV, while the overestimation drops to ∼7% for plasma of $\kappa = 7$ and $T = 60$ eV. For the same bulk energy, the temperature is overestimated by up to ∼12% when $T = 10$ eV and underestimated by the same order of magnitude when $\kappa = 2$. Both parameters approach the input values for higher κ and T (see also Figure 6). For higher κ and T the distribution function has a broader shape within the instrument's energy and angular bins. The discrete distribution function obtained from counts, therefore, represents more accurately the underlying continuous distribution.

(iii) Counting statistics cause an additional deviation (statistical error) between the fit results and the parameters of the underlying distribution (see Figure 7). Since this counting uncertainty follows the Poisson statistics, the accuracy of the output increases with the number of counts of the analyzed sample. In cases with an insufficient number of counts, we suggest (a) adding the measurements of consecutive samples or (b) adding the measurements obtained in consecutive energy channels to lower the Poisson error. We note, however, that in both cases an additional error is introduced (a) through potential temporal variations of the plasma or (b) through the reduction in energy resolution.

The method gives reliable and fast estimates for the expected observations from SWA-PAS and is, therefore, a potentially useful tool for on-board and/or ground processing of SWA-PAS observations. We note that, when automated for on-board processing, a minimal additional computational effort is required for the detection of the distribution's peak. In the case of SWA-PAS, such an algorithm is already in place in order to allow the instrument to take 3D measurements over a limited parameter space centered on the peak of the count rate distribution, precisely to save telemetry. SWA-PAS also has deployable modes in which the distribution is scanned in a limited (or even single) angular range in one spatial direction. The specific modes, trade angular coverage for temporal resolution, allowing very fast 1D measurements that are needed for some of the science goals of the mission (e.g., turbulence physics). Our method can provide the information on how the distributions evolve (in one spatial dimension) on these small timescales. In general, our method applies to any instrument with the same detection principle as SWA-PAS (e.g., the Ion Composition Analyzer on board Rosetta (Nilsson et al. 2007) or the Ion Mass Analyzer on Mars and Venus Express (Barabash et al. 2006, 2007)). The total error, however, depends on the plasma parameters and the instrument's characteristics such as its angular and energy resolution. Therefore, a careful validation for each individual instrument would be necessary in the way shown for the SWA-PAS design in Section 3.

As a first attempt to analyze existing plasma data similar to the artificial SWA-PAS data, we apply our method to *Helios* proton observations. We identify three examples of almost isotropic distributions published in the literature and derive the kappa indexes and temperatures with our method. The derived values are compared with those provided in the literature and the values we derive by fitting the entire 3D distribution function. For the large value of kappa found in distribution G, the shape of the distribution is nearly independent of its exact value. The temperatures derived by our method lie within a 20% margin of those derived by 3D fits to the distributions. It is possible that the amount of this misestimate lies within the error expected for the instrument (systematic and statistical), which is quantifiable with the methods presented in Section 3 for SWA-PAS. We also compare the derived temperatures with the values given by M82. The derived temperatures for distribution G lie within 5% of the temperatures derived by M82. In the case of distribution F, the temperature derived by our method and by the 3D fit is higher than the temperature derived from the moments calculation by M82. A possible explanation for this deviation is the tail contribution to the temperature at times when it is not fully observed due to instrumental sensitivity limitations. Therefore, the moment calculation results in a lower temperature than the actual temperature of the plasma. For distribution C2, our method and the 3D fit yield lower temperatures than the temperature derived from the moment integration. We note that the fitting techniques consider a specific and smooth expression for the distribution, whereas the moment integration does not. Therefore, deviations of the actual distribution from our analytical assumptions can lead to additional discrepancies between both approaches.

We note that our method provides an estimate of the kappa index and the plasma temperature in the direction vertical to the instrument's azimuth plane. Therefore, in the case of anisotropic plasma distributions, the estimated κ_{1D} likely has a value between $\kappa_{||}$ and $\kappa_{\perp}$, while the estimated T_{1D} has a value between $T_{||}$ and $T_{\perp}$, where the indexes represent the directions parallel and perpendicular to the magnetic field, respectively. However, even in these cases, the derived parameters can have a scientific value, especially if they can be returned at a higher cadence than the full 3D distribution data set.

We finally note that we have also used the MLE method to analyze the reduced 1D elevation profiles of the distribution function and compared with the results obtained by the fitting method. The comparison shows that both methods derive essentially the same results over a wide range of the input plasma parameters, but there is a deviation in the range of cold ($T <$ 20 eV) and low kappa index ($\kappa < 3$) plasma. In these cases, the fitting method estimates the temperature and kappa index closer to their input values. While future users may use alternative methods to analyze the reduced 1D elevation profiles, we advise that any method should be validated accordingly.

G.N. and C.J.O. are supported by the STFC Consolidated Grant to UCL/MSSL, ST/N000722/1. D.V. is supported by an STFC Ernest Rutherford Fellowship. The authors thank Dr. Colin Forsyth for helpful discussions.

ORCID iDs

G. Nicolaou https://orcid.org/0000-0003-3623-4928
G. Livadiotis https://orcid.org/0000-0002-7655-6019
C. J. Owen https://orcid.org/0000-0002-5982-4667
D. Verscharen https://orcid.org/0000-0002-0497-1096
R. T. Wicks https://orcid.org/0000-0002-0622-5302

References

Baluku, T. K., Hellberg, M. A., Kourakis, I., & Saini, N. S. 2010, PhPl, 17, 053702
Barabash, S., Lundin, R., Andersson, H., et al. 2006, SSRv, 126, 113

Barabash, S., Sauvaud, J. A., Gunell, H., et al. 2007, P&SS, 55, 1772
Carbary, J. F., Kane, M., Mauk, B. H., & Krimigis, S. M. 2014, JGRA, 119, 8426
Chotoo, K., Schwadron, N. A., Mason, G. M., et al. 2000, JGR, 105, 23107
Christon, S. P. 1987, Icar, 71, 448
Collier, M. R., & Hamilton, D. C. 1995, GeoRL, 22, 303
Decker, R. B., & Krimigis, S. M. 2003, AdSpR, 32, 597
Decker, R. B., Krimigis, S. M., Roelof, E. C., et al. 2005, Sci, 309, 2020
Dialynas, K., Krimigis, S. M., Mitchell, D. G., et al. 2009, JGRA, 114, A01212
Elliott, H. A., McComas, D. J., Valek, P., et al. 2016, ApJS, 223, 19
Elrod, M. K., Tseng, W.-L., Wilson, R. J., & Johnson, R. E. 2012, JGRA, 117, A03207
Eslami, P., Mottaghizadeh, M., & Pakzad, H. R. 2011, PhPl, 18, 102303
Fisk, L. A., & Gloeckler, G. 2014, JGRA, 119, 8733
Heerikhuisen, J., Pogorelov, N. V., Florinski, V., Zank, G. P., & le Roux, J. A. 2008, ApJ, 682, 679
Heerikhuisen, J., Pogorelov, N. V., Zank, G. P., et al. 2010, ApJL, 708, L126
Heerikhuisen, J., Zirnstein, E., & Pogorelov, N. 2015, JGRA, 120, 1516
Hellberg, M. A., Mace, R. L., Baluku, T. K., Kourakis, I., & Saini, N. S. 2009, PhPl, 16, 094701
Jurac, S., McGrath, M. A., Johnson, R. E., et al. 2002, GeoRL, 29, 2172
Kasper, J. C., Lazarus, A. J., Steinberg, J. T., Ogilvie, K. W., & Szabo, A. 2006, JGRA, 111, A03105
Kletzing, C. A., Scudder, J. D., Dors, E. E., & Curto, C. 2003, JGRA, 108, 1360
Kourakis, I., Sultana, S., & Hellberg, M. A. 2012, PPCF, 54, 124001
Lawless, J. F. 2011, Statistical Models and Methods for Lifetime Data (2nd ed.; New York: Wiley)
Le Roux, J. A., Webb, G. M., Shalchi, A., & Zank, G. P. 2010, ApJ, 716, 671
Leubner, M. P. 2002, Ap&SS, 282, 573
Liu, H.-F., Tanga, C.-J., Zhanga, X., Zhua, L.-M., & Zhao, Y. 2015, AdSpR, 56, 2298
Livadiotis, G. 2009, JMaCh, 45, 930
Livadiotis, G. 2014, Entrp, 16, 4290
Livadiotis, G. 2015a, JGRA, 120, 1607
Livadiotis, G. 2015b, JGRA, 120, 880
Livadiotis, G. 2015c, Entrp, 17, 2062
Livadiotis, G. 2016a, PhyA, 445, 240
Livadiotis, G. 2016b, EL, 113, 10003
Livadiotis, G. 2017, Kappa Distributions: Theory and Applications in Plasmas (Amsterdam: Elsevier)
Livadiotis, G., & McComas, D. J. 2009, JGRA, 114, A11105
Livadiotis, G., & McComas, D. J. 2010a, ApJ, 714, 971
Livadiotis, G., & McComas, D. J. 2010b, PhyS, 82, 035003
Livadiotis, G., & McComas, D. J. 2011a, ApJ, 738, 64
Livadiotis, G., & McComas, D. J. 2011b, ApJ, 741, 88
Livadiotis, G., & McComas, D. J. 2012, ApJ, 749, 11
Livadiotis, G., & McComas, D. J. 2013a, SSRv, 75, 183
Livadiotis, G., & McComas, D. J. 2013b, JGRA, 118, 2863
Livadiotis, G., & McComas, D. J. 2013c, Entrp, 15, 1118
Livadiotis, G., McComas, D. J., Dayeh, M. A., Funsten, H. O., & Schwadron, N. A. 2011, ApJ, 734, 1
Livadiotis, G., McComas, D. J., Randol, B. M., et al. 2012, ApJ, 751, 64
Livadiotis, G., McComas, D. J., Schwadron, N. A., Funsten, H. O., & Fuselier, S. A. 2013, ApJ, 762, 134
Livi, R. J., Burch, J. L., Crary, F., et al. 2014, JGRA, 119, 3683
Maksimovic, M., Pierrard, V., & Rilay, P. 1997, GeoRL, 24, 1151
Maksimovic, M., Zouganelis, I., Chaufray, J. Y., et al. 2005, JGRA, 110, A09104
Mann, G., Classen, H. T., Keppler, E., & Roelof, E. C. 2002, A&A, 391, 749
Marsch, E. 2006, LRSP, 3, 1
Marsch, E., Mühlhäuser, K.-H., Schwenn, R., et al. 1982, JGR, 87, 52
Mauk, B. H., Mitchell, D. G., McEntire, R. W., et al. 2004, JGR, 109, A09S12
Milovanov, A. V., & Zelenyi, L. M. 2000, NPGeo, 7, 211
Nicolaou, G., & Livadiotis, G. 2016, Ap&SS, 361, 359
Nicolaou, G., McComas, D. J., Bagenal, F., & Elliott, H. A. 2014, JGRA, 119, 3463
Nicolaou, G., McComas, D. J., Bagenal, F., Elliott, H. A., & Ebert, R. W. 2015a, P&SS, 111, 116
Nicolaou, G., McComas, D. J., Bagenal, F., Elliott, H. A., & Wilson, R. J. 2015b, P&SS, 119, 222
Nilsson, H., Lundin, R., Lundin, K., et al. 2007, SSRv, 128, 671
Ogasawara, K., Angelopoulos, V., Dayeh, M. A., et al. 2013, JGRA, 118, 3126
Paschmann, G., & Daly, P. W. 1998, Methods for Multi-Spacecraft Data, Vol. 1, ISSI Scientific Report Series SR-001 (Paris: ESA)
Pierrard, V., Maksimovic, M., & Lemaire, J. 1999, JGR, 104, 17021
Pierrard, V., & Pieters, M. 2014, JGRA, 119, 9441
Pisarenko, N. F., Budnika, E. Y., Ermolaev, Y. I., et al. 2002, JASTP, 64, 573
Qureshi, M. N. S., Nasir, W., Masood, W., et al. 2014, JGRA, 119, 059
Raadu, M. A., & Shafiq, M. 2007, PhPl, 14, 012105
Randol, B. M., & Christian, E. R. 2014, JGRA, 119, 7025
Richardson, J. D. 1987, JGR, 92, 6133
Richardson, J. D. 2002, P&SS, 50, 503
Rosenbauer, H., Schwenn, R., Marsch, E., et al. 1977, JGZG, 42, 561
Saito, S., Forme, F. R. E., Buchert, S. C., Nozawa, S., & Fujii, R. 2000, AnGeo, 18, 1216
Scherer, K., Fahr, H. J., Fichtner, H., et al. 2018, AnGe, 36, 37
Schippers, P., Blanc, M., Andre, N., et al. 2008, JGRA, 113, A07208
Schwenn, R., Rosenbauer, H., & Miggenrieder, H. 1975, RF, 19, 226
Stepanova, M., & Antonova, E. E. 2015, JGRA, 120, 3702
Štverák, Š., Maksimovic, M., Trávníček, P. M., et al. 2009, JGRA, 114, A05104
Tribeche, M., Mayout, S., & Amour, R. 2009, PhPl, 16, 043706
Tsallis, C. 1988, JSP, 52, 479
Tsallis, C. 2009, Introduction to Nonextensive Statistical Mechanics: Approaching a Complex World (New York: Springer)
Tsallis, C., Mendes, R. S., & Plastino, A. R. 1998, PhyA, 261, 534
Varotsos, P. A., Sarlis, N. V., & Skordas, E. S. 2014, JGRA, 119, 9192
Viñas, A. F., Moya, P. S., Navarro, R. E., et al. 2015, JGRA, 120, 3307
Wilson, R. J., Bagenal, F., Delamere, P. A., et al. 2013, JGRA, 118, 2122
Wilson, R. J., Crary, F., Gilbert, L. K., et al. 2012a, PDS User's Guide for Cassini Plasma Spectrometer (CAPS), Planetary Data System, http://ppi.pds.nasa.gov/
Wilson, R. J., Delamere, P. A., Bagenal, F., & Masters, A. 2012b, JGRA, 117, A03212
Wilson, R. J., Tokar, R. L., Henderson, M. G., et al. 2008, JGRA, 113, A12218
Yoon, P. H. 2014, JGRA, 119, 7074
Yoon, P. H., Rhee, T., & Ryu, C. M. 2006, JGRA, 111, A09106
Zank, G. P., Heerikhuisen, J., Pogorelov, N. V., Burrows, R., & McComas, D. J. 2010, ApJ, 708, 1092
Zouganelis, I., Maksimovic, M., Meyer-Vernet, N., Lamy, H., & Issautier, K. 2004, ApJ, 606, 542